fluids

MDPI

Article

Rarefied Nozzle Flow Computation Using the Viscosity-Based Direct Simulation Monte Carlo Method

Deepa Raj Mopuru [1], Nishanth Dongari [2,*] and Srihari Payyavula [3]

[1] Defence Research & Development Laboratory, Kanchanbagh, Hyderabad 500058, India; me14resch11012@iith.ac.in
[2] Department of Mechanaical & Aerospace Engineering, Indian Institute of Technology, Hyderabad, Sangareddy 502285, India
[3] Research Centre Imarat, Vigyanakancha, Hyderabad 500069, India; psrihari@hotmail.com
* Correspondence: nishanth@mae.iith.ac.in

Abstract: Micro-nozzles are essential for enabling precise satellite attitude control and orbital maneuvers. Accurate prediction of performance parameters, including thrust and specific impulse, is critical, necessitating careful design of these nozzles. Given the high Knudsen numbers associated with micro-nozzle flows, rarefied gas dynamics often dominate, and conventional computational fluid dynamics (CFD) methods fail to capture accurate flow expansion behavior. The Direct Simulation Monte Carlo (DSMC) method, developed by Bird, is widely used for modeling rarefied flows; however, it has been primarily implemented on platforms like OpenFOAM and FORTRAN, with limited exploration in MATLAB. This study presents the development of a viscosity-based DSMC (μDSMC) simulation framework in MATLAB for analyzing rarefied gas expansion through micro-nozzles. Key boundary conditions, including upstream and downstream pressure conditions and thermal wall treatments with diffuse reflection, are incorporated into the code. The μDSMC results are validated against traditional DSMC outcomes, showing strong agreement. Grid convergence studies indicate that the radial grid size must be less than one-third of the mean free path, with a more relaxed requirement on axial grid size. Flow characteristics within micro-nozzles are evaluated across varying ambient pressures and gas species in terms of the back pressure ratio, effective exit flow ratio, and exit flow velocity. Studies indicated that a minimum back pressure ratio is required, beyond which the effective nozzle flow expansion is achieved. Parametric analysis further suggests that gases with lower molecular weights are preferable for achieving optimal expansion in micro-nozzles under low ambient pressures.

Keywords: rarefied flow expansion; micro-nozzle; DSMC; MATLAB; variable hard sphere; attitude control

check for updates

Academic Editors: Ramesh Agarwal, V'yacheslav Akkerman and Lin Tian

Received: 14 September 2024
Revised: 14 November 2024
Accepted: 12 December 2024
Published: 24 December 2024

Citation: Mopuru, D.R.; Dongari, N.; Payyavula, S. Rarefied Nozzle Flow Computation Using the Viscosity-Based Direct Simulation Monte Carlo Method. *Fluids* **2025**, *10*, 2. https://doi.org/10.3390/fluids10010002

Copyright: © 2024 by the authors. Licensee MDPI, Basel, Switzerland. This article is an open access article distributed under the terms and conditions of the Creative Commons Attribution (CC BY) license (https://creativecommons.org/licenses/by/4.0/).

1. Introduction

Recent technical demands of launching multiple satellites in a single spacecraft have been observed, leading to the development of many smaller satellites. The Attitude Control System (ACS) for a satellite is an essential auxiliary propulsive element that provides attitude control and orbit maneuver capability to the satellite. The ACS employs thrusters as its main key element, which are operated on demand by pulsing them at the required frequency. The performance parameters of the ACS thruster like thrust, combustion efficiency, and impulse bit need to be accurately determined. Due to the high altitude of operation and also due to the low weight of the satellite, low thrust is sufficient for

providing a reaction/moment or roll rate to the satellite, leading further to the design of a milli-nozzle or micro-nozzle that can operate at low chamber pressures and temperatures. Utmost care has to be taken during the design of a micro-nozzle as the flow is characterized by the Knudsen number (Kn), which decides the degree of rarefaction in gas. It is defined as the ratio of the mean free path (λ) to the characteristic length scale (L). Fluid flow is divided into the following regimes on the basis of the Knudsen number: (a) continuum regime ($Kn \leq 0.001$); (b) slip flow regime ($0.001 < Kn < 0.1$); (c) transition flow ($0.1 \leq Kn \leq 10$); (d) free molecular flow ($Kn > 10$).

Flow expansion through any nozzle can go through a continuum regime to a highly rarefied flow depending on its operating conditions, nozzle geometry, and type of gas. As the characteristic length scale is very low in a micro-nozzle—and also due to the high surface-area-to-volume ratio—viscous effects tend to dominate, resulting in lower Reynolds numbers. Conventional nozzle flow relations are no longer valid in micro-nozzle cases since the assumptions of the Inviscid Flow model are invalid. The effect of a lower Reynolds number, leading to a thicker boundary layer—especially in the divergent section of the nozzle—has direct implications on the effective exit flow ratio, which is a deciding parameter for the thrust delivered by the thruster. Further, due to the low Reynolds number and high Mach number in a micro-nozzle, the flow expanding through it is highly rarefied.

As the flow becomes rarefied, there is an insufficient number of collisions between the particles, resulting in a thermal non-equilibrium—due to which the conventional CFD framework is not applicable [1]. The conventional CFD framework, considering the Navier–Stokes–Fourier constitutive relations with no-slip and no-jump boundary conditions for the velocity and temperature, respectively, tends to fail when the validity of the continuum analysis is doubtful. Predictions obtained from the mentioned framework may sometimes lead to an overdesign of the micro-nozzle, resulting in inaccurate results for the performance parameters. Hence, it is essential to use the Direct Simulation Monte Carlo (DSMC) method because it is the most accurate method for predicting flow behavior at high Knudsen numbers.

DSMC was initially proposed by Bird [1] and has been employed in various studies related to MEMS and re-entry vehicles where the effect of the low characteristic length scale and lower gas density is predominant. The DSMC method is a probabilistic approach where the flow is represented by a large number of DSMC particles and the flow evolves by calculating the motion of these particles and their collisions amongst themselves as well as with boundaries. The main requirements of the DSMC approach in order to obtain an accurate solution are (a) to have a time-step size much lower than the local mean collision time so that transport and collision phases are decoupled; (b) to have a grid size much less than the local mean free path; (c) to have a sufficiently large number of DSMC particles in each cell, to ensure accurate statistical representation during the collision phase [2]. In this paper, a simplistic approach by Macrossan [3] termed the viscosity-based DSMC (μDSMC) method is presented, by which an arbitrary viscosity law can be implemented. In this method, the collision cross-section is computed on a cell-by-cell basis based on time-averaged kinetic temperature and viscosity defined at that temperature. This approach was modeled by Macrossan [3] for a high-speed Couette flow with a hard sphere collision model and compared against the standard DSMC method by Bird, ultimately reproducing the variation in viscosity given by any arbitrary law. It is as simple as the standard DSMC method, and the computational border required to achieve an arbitrary viscosity law is negligible [3]. In this paper, this approach is extended to two-dimensional flows with a variable hard sphere collision model along with necessary boundary conditions.

It is also essential to implement proper boundary conditions in the DSMC method in order to obtain an accurate solution. Various types of boundary conditions are used for DSMC simulations, including periodic boundary conditions, specular reflection, diffuse

reflection, stream and vacuum boundary conditions, etc. In order to model flow expansion through a micro-nozzle by the DSMC method, where walls are at an angle w.r.t flow, diffuse-reflection-type boundary conditions are modified to take into account the effect of the slantness of the wall. At the upstream of a micro-nozzle, a stream-type boundary condition can be implemented only if information about density, velocity, and temperature is known in advance. When the flow is subsonic at the inlet of the nozzle and known values are only gas properties, a stream boundary condition cannot be implemented. At the downstream of a micro-nozzle, a vacuum-type boundary condition cannot be implemented as it operates with a finite back pressure. These limitations at the upstream and downstream of a nozzle are overcome by applying a pressure-based boundary condition approach based on the characteristic theory [4–7].

In this paper, the viscosity-based DSMC (μDSMC) approach by MN Macrossan [3] is explained and extended to variable hard sphere gas expanding through micro-nozzle geometry, which was experimentally investigated by Hao [8], along with relevant boundary conditions. All the numerical procedures related to the μDSMC approach are modeled in MATLAB (https://www.mathworks.com/products/matlab.html (accessed on 13 September 2024)) and are compared against the traditional DSMC approach results by Jaiswal [9], which were modeled using the dsmcFOAM solver in OpenFOAM (https://openfoam.org/ (accessed on 13 September 2024)).

The agenda of this paper is as follows: Section 2 presents a brief overview of the numerical simulation method employed for μDSMC, Section 3 discusses the collision model employed in μDSMC, Section 4 presents details on the simulation carried out on the available micro-nozzle, Section 5 presents results obtained from μDSMC approach and a comparison with standard DSMC approach, Section 6 discusses nozzle flow expansion behavior for different gas species and for different ambient pressures, and Section 7 presents the conclusions of this paper.

2. Numerical Method

The Direct Simulation Monte Carlo (DSMC) method by Bird is a standard way of modeling rarefied flows, where the governing equation is the Boltzmann equation. In the DSMC method, flow is represented by a large number of DSMC particles, and the flow is computed by calculating the motion of these particles and their interaction with themselves as well as with boundaries.

Each DSMC particle represents a large number of real molecules. The flow chart of the DSMC process is detailed in Figure 1 and mainly consists of the following processes.

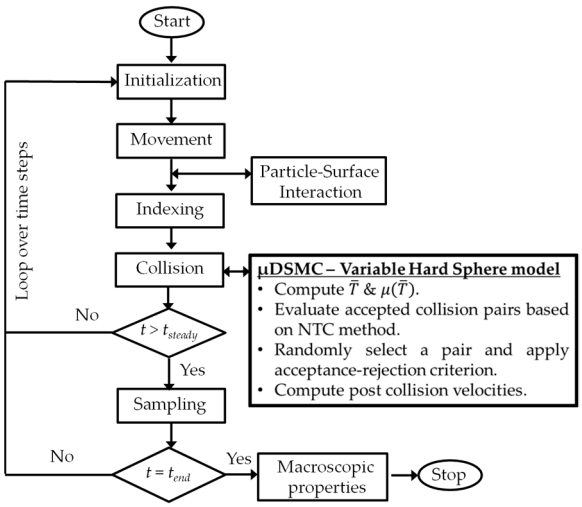


Figure 1. Flow chart of μDSMC method.

2.1. Initialization

Initially, the computational domain is filled with DSMC particles. Before the μDSMC simulation is started, the whole computational domain is initialized and divided into N_x cells along the axial direction and N_y cells along the radial direction. The basic definitions of the initialization process are explained briefly with a formulation in Appendix A. The basic rule of thumb for the DSMC method is that cell size should be less than or equal to one-third of the mean free path, especially for radial direction. The discrete time step is evaluated such that it is much less than the mean collision time. Initially, an equal number of DSMC particles per cell (in the current case, 20 DSMC particles per cell are considered) are distributed randomly based on ambient pressure conditions. The velocities of each particle in the domain are randomly assigned according to Maxwellian equilibrium distribution as mentioned by Bird [1].

2.2. Particle Movement

During each discrete time step, particles are moved inside the domain using the assigned molecular velocities. The basic rule of thumb of the time step being much less than the mean collision time is followed, so as to decouple molecular collision during the particle movement. Particle–surface interaction is modeled by assigning the respective boundary condition procedures:

- Diffusive reflection with the thermal wall oriented vertically and the other wall oriented at the required slant angle;
- Specular reflection for the axi-symmetric type of boundary condition;
- Implicit pressure-based boundary conditions at the upstream and downstream boundaries.

2.3. Sorting of Particles

After the particle–surface interaction is modeled, the total number of particles per cell and the respective particle index numbers are evaluated for every cell in the domain. A function file for sorting the particles in each cell is written in MATLAB using the built-in function *'find'* in order to find the total number of particles in each cell.

2.4. Collision Model

The variable hard sphere collision model is chosen such that the collision cross-section is based on viscosity defined at the time-averaged temperature ($\overline{T}$) in each cell. The total number of accepted collision pairs 'N_{coll}' is evaluated based on the no-time-counter (NTC) method by Bird [1]. A potential pair of collision partners is chosen at random from particles within the cell, and the pair is accepted based on the acceptance–rejection criteria of the product of the collision cross-section area and the relative velocity of the pair. If the pair is accepted, the post-collision velocities are evaluated and updated for the respective particles. This process of selection and acceptance of collision pairs is repeated until all potential 'N_{coll}' collision pairs are processed. This is further detailed in Section 3 on the variable hard sphere collision model.

2.5. Sampling for Macroscopic Properties

Sampling for macroscopic properties is performed after the steady state is reached and is performed for molecular velocity information in each cell of the computational domain. For a particular cell under consideration, data like the cumulative sum of particles, particle velocities, and squared velocities of particles are computed at each time step after the steady state of time. All the macroscopic properties are further computed from the attained data.

The viscosity-based DSMC approach (μDSMC) with all relevant boundary conditions is modeled in detail using the MATLAB platform with the help of inputs from [10,11], and

it is applied for two-dimensional flow expanding through a micro-nozzle at a particular background pressure. The simulation results are compared with the traditional DSMC results given by Jaiswal [9]. The MATLAB platform is chosen for its user-friendly interface and its built-in functions. A parametric study with numerous DSMC simulations is made easier with the parallel computing options in the MATLAB platform.

3. Variable Hard Sphere Collision Model—μDSMC Approach

The most common collision model used so far in the DSMC method is the variable hard sphere model (VHS) where the total collision cross-section varies with the relative velocity of collisions, given by Equation (1) as

$$\sigma(g) = \sigma_{ref}\left(\frac{g_{ref}}{g}\right)^{2\nu} \tag{1}$$

where g_{ref} and σ_{ref} are the reference values of the collision speed and total cross-section, respectively, and ν is a constant related to the viscosity exponent (ω) of gas given by Equation (2) as

$$\nu = \omega - \frac{1}{2} \tag{2}$$

The Chapman–Enskog viscosity for a collection of VHS particles is given by [1] Equation (3) as

$$\mu = \frac{15m}{8\Gamma(4-\nu)}\frac{\sqrt{\pi RT}(4RT)^{\nu}}{\sigma_{ref}\left(g_{ref}\right)^{2\nu}} \tag{3}$$

where Γ is a gamma function. Macrossan [3] described a simpler and faster DSMC approach named 'viscosity DSMC' or '*μDSMC*', by which a simple collision cross-section can be used to model any realistic viscosity law, including one based on empirical data. This is achieved by adjusting parameters in the collision model on a cell-by-cell basis based on the time-averaged kinetic temperature in each cell and the required viscosity at that temperature [3]. After the time-averaged kinetic temperature in each cell is computed, the dependence of viscosity on the temperature shall be chosen. For instance, if viscosity variation by Sutherland potential is chosen, then viscosity based on time-averaged kinetic temperature shall be as described in Equation (4):

$$\mu(\overline{T}) = \mu_{ref}\left(\frac{\overline{T}}{T_{ref}}\right)^{1.5}\frac{T_{ref}+T_s}{\overline{T}+T_s} \tag{4}$$

In Equation (4), $\overline{T}$ is the time-averaged kinetic temperature in each cell, T_s is a measure of the strength of the attractive potential, and μ_{ref} is the reference viscosity of gas known at reference temperature T_{ref}.

With a known variation in viscosity $\mu(\overline{T})$ and with the reference collision speed $g_{ref} = \sqrt{4R\overline{T}}$, the reference collision cross-section area can be evaluated as shown in Equation (5):

$$\sigma_{ref} = \frac{15m}{8\Gamma(4-\nu)}\frac{\sqrt{\pi R\overline{T}}}{\mu(\overline{T})} \tag{5}$$

The local value of collision cross-section area $\sigma(g_{max})$ is evaluated based on σ_{ref}, g_{ref}, and g_{max}, where g_{max} is an estimate of the maximum possible collision speed in the cell.

The 'accepted' number of collision pairs in the cell using Bird's standard no-time-counter (NTC) method is given by Equation (6) [1]:

$$N_{coll} = \frac{1}{2} F_N N_{pc} \left(N_{pc} - 1\right) g_{\max} \sigma(g_{\max}) \frac{\Delta t}{V_{cell}} \tag{6}$$

In Equation (6), N_{coll} is the accepted number of collisions in each cell, N_{pc} is the number of DSMC particles in the cell, Δt is the time step, V_{cell} is the cell volume, and F_N is the statistical weight. F_N is defined as the ratio of total real gas molecules to total DSMC particles and is shown in Equation (7):

$$F_N = \frac{n V_{domain}}{N_{dsmc}} \tag{7}$$

where n is the number density, V_{domain} is the volume of the domain, and N_{dsmc} is the total number of DSMC particles. Based on the acceptance–rejection criterion, a pair is accepted for collision if

$$\frac{g\sigma(g)}{g_{\max}\sigma(g_{\max})} > R_f \tag{8}$$

where R_f is a uniformly distributed random fraction and 'g' is the relative velocity between the collision pair of particles with velocities $\vec{c_1}$ and $\vec{c_2}$ which is given by $\vec{g} = \vec{c_1} - \vec{c_2}$. After the collision is accepted, post-collision velocities $\vec{c_1^*}$ and $\vec{c_2^*}$ are obtained by the conservation of momentum and energy, as detailed in Equations (9) and (10):

$$\vec{c_1^*} = \frac{\vec{c_1} + \vec{c_2}}{2} + \frac{\vec{g^*}}{2} \tag{9}$$

$$\vec{c_2^*} = \frac{\vec{c_1} + \vec{c_2}}{2} - \frac{\vec{g^*}}{2} \tag{10}$$

where $\vec{g^*}$ is the post-collision relative velocity between particles, and its components are given by Equation (11):

$$\vec{g^*} = |g|[(\cos\alpha)\vec{i} + (\sin\alpha\cos\phi)\vec{j} + (\sin\alpha\sin\phi)\vec{k}] \tag{11}$$

The post-collision relative velocity between particles can be evaluated by Equation (11) along with $cos\,\alpha = 1 - 2R_f$, $sin\,\alpha = \sqrt{1 - cos^2\alpha}$, and $\phi = 2\pi R_f$, where R_f is a random fraction uniformly distributed in [0, 1).

There are other efficient collision models that are used, like the Simplified Bernoulli Trial (SBT) collision scheme by Roohi [12], but the conventional no-time-counter (NTC) method is currently modeled on the MATLAB platform. The NTC method is still an efficient method for evaluating intermolecular collisions in all flow regimes having a Knudsen number greater than 0.01 [12].

4. Simulation Details

The viscosity-based DSMC approach outlined by Macrossan [3] was extended to two-dimensional flows with nitrogen as a working gas expanding in a micro-nozzle outlined by ABCC'B'A', as shown in Figure 2. The three major characteristic lengths of the micro-nozzle are the throat height (H_2) of 10 µm, exit height (H_3) of 17 µm, and inlet height (H_1) of 34 µm. The axial lengths of the micro-nozzle are the length from the inlet section to the throat (L_1), which is 50 µm, and the length from the throat to the exit section (L_2), which is 95 µm. The

external domain added to the micro-nozzle has a length (L_3) of 55 µm and height (H_4) of 25 µm. The line OO′ is the axi-symmetrical line of the nozzle under consideration.

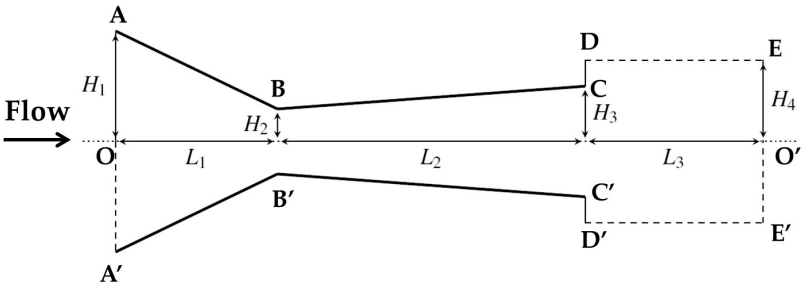


Figure 2. Computational domain of micro-nozzle.

With consideration of symmetry, the region name OABCDEO′ is simulated for nozzle flow expansion. The axi-symmetric boundary is modeled with specular reflection set to OO′. Two different kinds of boundary conditions can be considered for walls. One is at a constant temperature (300 K), and the other is an adiabatic wall. It has been found that the same results (of relative error < 1%) are obtained for different settings of wall conditions [13]. In the present case, diffusive reflection for a thermal wall at a constant temperature of 300 K is set for walls AB, BC, and CD. As walls AB and BC are at an angle w.r.t the axial direction, these walls need thermal boundary treatment for a slant wall. The convergent and divergent angles of the micro-nozzle can be computed from the nozzle dimensions and are given as input for thermal boundary treatment for a slant wall as per the procedure explained in Appendix B. At inlet OA, implicit upstream pressure boundary conditions are considered, and at outlet DE and EO′, implicit downstream pressure boundary conditions are considered.

Nitrogen is a working medium expanding through the above-mentioned micro-nozzle from an inlet pressure of 1576.8 Pa at a temperature of 300 K into ambient conditions of pressure 157.68 Pa. The number density corresponding to operating conditions is 3.807×10^{23} per m^3. The flow corresponds to a Knudsen number of 0.0502. The properties of nitrogen gas considered for the simulation are mentioned in Table 1.

Table 1. Properties of nitrogen gas.

m (kg)	μ_{ref} (Ns/m^2)	T_{ref} (K)	T_s (K)	ω	γ
4.65×10^{-26}	1.652×10^{-5}	273	111	0.74	1.4

Before the µDSMC simulation is started, the whole computational domain 'OAFO' is initialized at ambient pressure conditions. The computational domain filled with DSMC particles is shown in Figure 3. The domain is divided into N_x cells along the axial direction and N_y cells along the radial direction. The particles in the cells bounded by ABCDEFA are discarded using the *'find'* function in MATLAB and are not considered for particle movement or collisions. The velocities of each particle in the domain are randomly assigned according to Maxwellian equilibrium distribution as mentioned by Bird [1].

The chosen number of cells in the domain is 70 cells along the axial direction and 30 cells along the radial direction. Corresponding grid sizes are 0.84λ along the axial direction and 0.33λ along the radial direction, where 'λ' is the mean free path computed for variable hard sphere molecular gas. In the current simulation case, the time step considered is $0.1\tau_{vhs}$, where τ_{vhs} is the mean collision time evaluated for variable hard sphere molecular gas. A steady state was well established after an elapsed time of $\frac{100L_y}{\overline{c'}}$. Sampling for macroscopic properties is performed for elapsed time in the interval $\frac{100L_y}{\overline{c'}} \leq t \leq \frac{300L_y}{\overline{c'}}$. The

grid independence studies along the radial and axial directions are carried out, and results are given in detail in the subsequent section. Simulations for time-step independence and particles-per-cell independence are also carried out. Further, the results are compared with those for the standard DSMC case presented by Jaiswal [9].

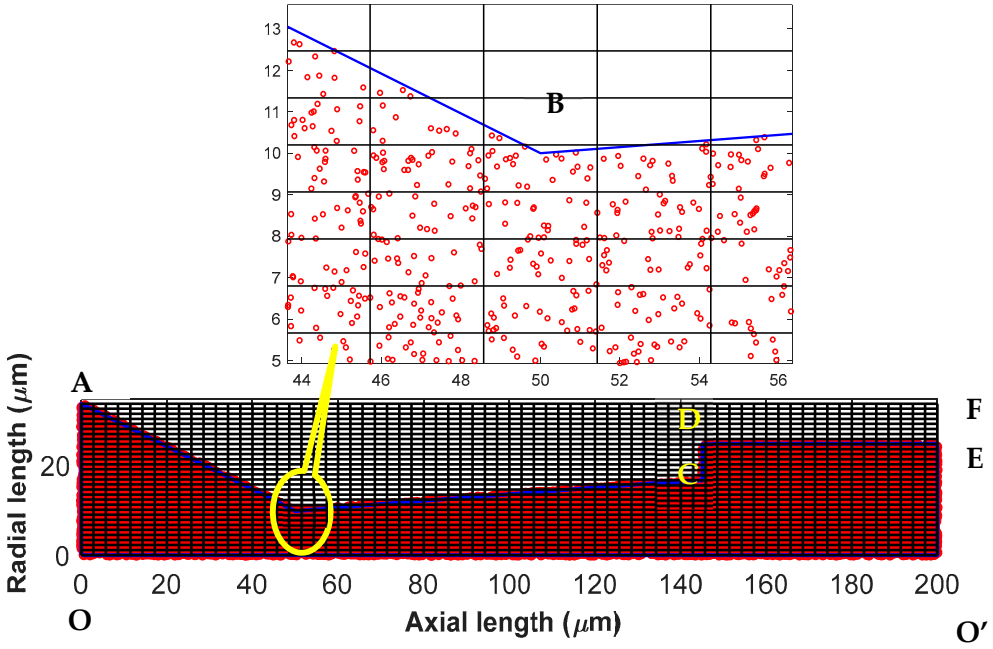


Figure 3. Computational domain with DSMC particles.

5. Results and Discussion

The computational intensiveness of the DSMC method depends on the total number of DSMC particles, which in turn is decided by the number of cells and the number of particles per cell. Therefore, it is essential to study the effect of the total number of cells, the number of particles per cell, and the size of the time step in order to prevent an unnecessary rise in computational cost.

5.1. Radial Grid Size Independence Studies

Grid size independence studies are carried out for radial grid sizes (Δy) varying from 0.25λ to 1λ. The fixed parameters are axial grid size (Δx) as 0.84λ, time step (dt) as one-tenth of the mean collision time, and particles per cell (ppc) as 20 particles. A comparison of the results for the center-line Mach number and normalized pressure for varying radial grid sizes is shown in Figure 4a,b, respectively. It can be observed that the results for grid sizes $0.84\lambda \times 0.25\lambda$, $0.84\lambda \times 0.33\lambda$, and $0.84\lambda \times 0.5\lambda$ are in closer agreement with each other than with those of a coarser grid, $0.84\lambda \times 1\lambda$. Further, the Mach number at the exit plane is compared for the mentioned grid sizes in Figure 5, indicating significant convergence of results between the grid sizes of $0.84\lambda \times 0.25\lambda$ and $0.84\lambda \times 0.33\lambda$. The grid size of $0.84\lambda \times 0.33\lambda$ is considered as the final grid size in order to save on the computational cost.

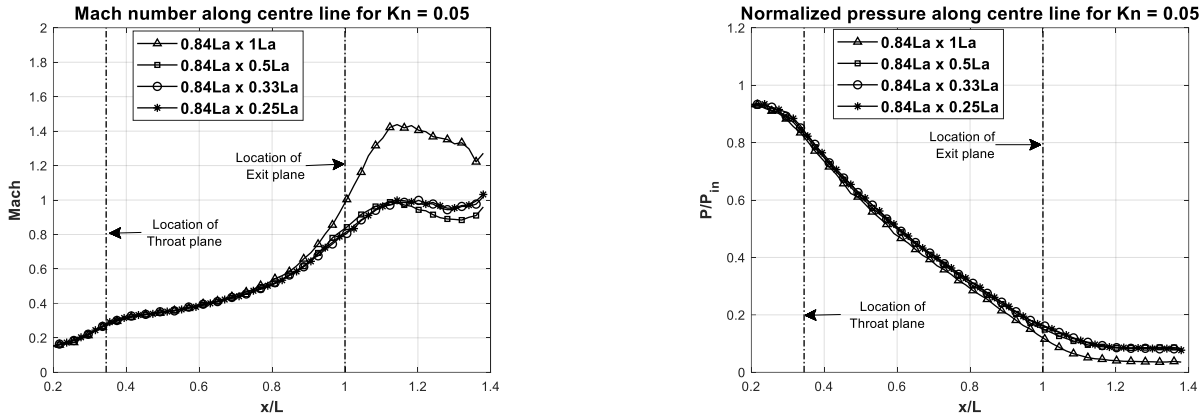


Figure 4. Radial grid independence studies for (**a**) center-line Mach number and (**b**) center-line normalized pressure.

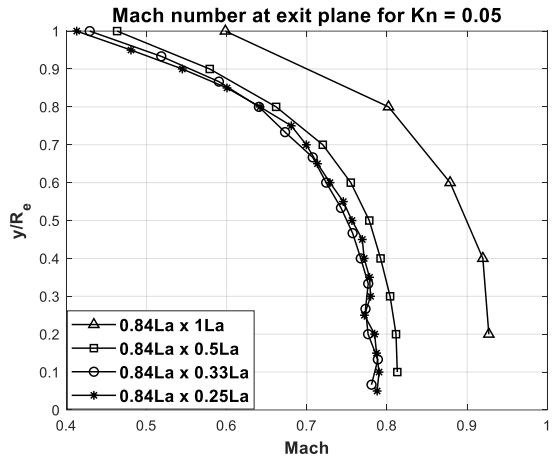
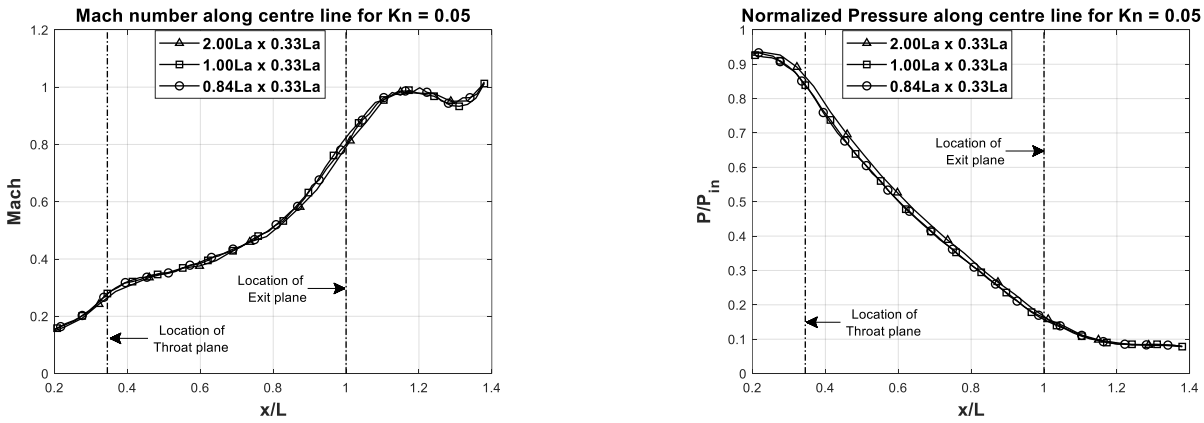


Figure 5. Radial grid independence studies for exit Mach number.

5.2. Axial Grid Size Independence Studies

Grid size independence studies are carried out for axial grid sizes (Δx) varying from 0.84λ to 3λ. The fixed parameters are radial grid size (Δy) as 0.33λ, time step (dt) as one-tenth of the mean collision time, and particles per cell (ppc) as 20 particles. A comparison of the results for the center-line Mach number and normalized pressure for varying axial grid sizes is shown in Figure 6a,b, respectively. It can be observed that results are in close match irrespective of axial grid size. As the flow does not experience major gradients along the axial direction, the results are expected to be independent of axial grid size. It has also been highlighted by Roohi et al. [12] that sufficient numerical accuracy is still achievable with a smaller number of cells along with the major advantage of a reduction in computational time. Based on the results from Figures 4 and 5, the grid size corresponding to $0.84\lambda \times 0.33\lambda$ is chosen as the final grid size. Additional computational time may be avoided if the grid size corresponding to $1.00\lambda \times 0.33\lambda$ is chosen, but for an accurate flow simulation, $0.84\lambda \times 0.33\lambda$ is chosen as the final grid size. It may also be concluded that it is sufficient to maintain a radial grid size (Δy) of the order less than or equal to one-third of the mean free path. Further, it is sufficient if the axial grid size (Δx) is maintained such that It Is less than the mean free path.

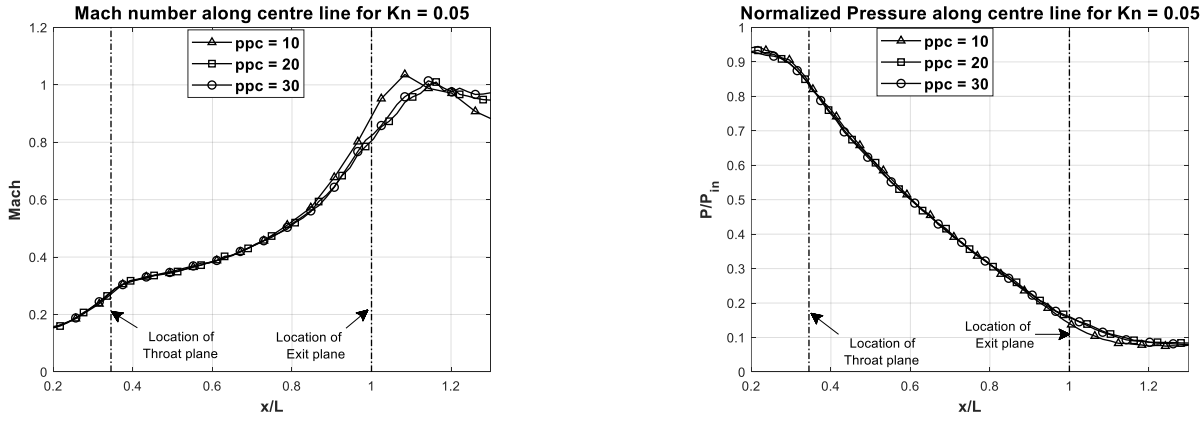


(**a**) (**b**)

Figure 6. Axial grid independence studies for (**a**) center-line Mach number and (**b**) center-line normalized Pressure.

5.3. Particles-per-Cell Independence Studies

Particles per cell (*ppc*) independence studies are carried out, varying from 10 particles to 30 particles for a domain with a grid size of $0.84\lambda \times 0.33\lambda$ and a time step that is one-tenth of the mean collision time. A comparison of results for the center-line Mach number and normalized pressure for varying particles per cell is shown in Figure 7a,b, respectively. This might be attributed to the effect of statistical weight (F_N) on the number of collision pairs evaluated. Upon further examination, simulations with 20 and 30 particles per cell predict closer solutions than those with 10 particles per cell. In conclusion, the computational cost could be further reduced if 20 particles per cell is chosen.



(**a**) (**b**)

Figure 7. Particles-per-cell independence studies for (**a**) center-line Mach number and (**b**) center-line normalized pressure.

5.4. Time-Step Independence Studies

Time-step independence studies are carried out, with a step size varying from as low as $0.02\tau_{vhs}$ to as high as $0.4\tau_{vh}$s for a domain with a grid size of $0.84\lambda \times 0.33\lambda$ and 20 particles per cell. For reference, a comparison of results for cases with time-step sizes $0.02\tau_{vhs}$, $0.1\tau_{vhs}$, $0.15\tau_{vhs}$, and $0.4\tau_{vhs}$ is shown in Figure 8a,b. From the set of results, it can be concluded that the time step should not be too high or too low. When the time-step size was as low as $0.02\tau_{\mathrm{vhs}}$, nozzle flow expansion was incomplete within the elapsed time of $t = \frac{300L_y}{c'}$. It was also observed that the recirculation flow at the vertical wall CD was well established and was clearer for step sizes of $0.1\tau_{vhs}$ and $0.15\tau_{vhs}$ than for step sizes of

$0.02\tau_{vhs}$ and $0.4\tau_{vhs}$. Clearly, these recirculation zones were not captured when the time step was greater than $0.3\tau_{vhs}$. So, from time-step independence studies, it can be concluded that the optimum step size is $0.1\tau_{vhs}$, i.e., one-tenth of the mean collision time.

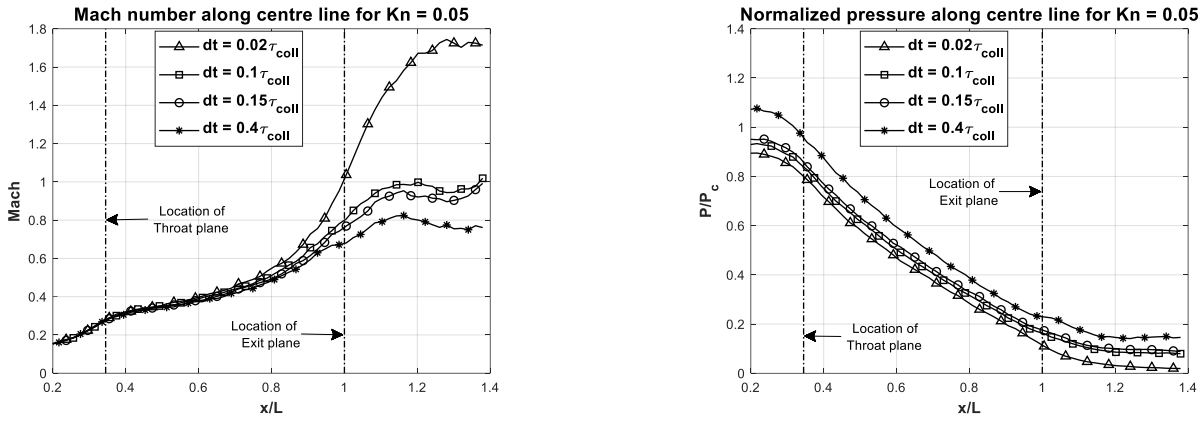


Figure 8. Time-step independence studies for (**a**) center-line Mach number and (**b**) center-line normalized pressure.

5.5. Comparison with Standard DSMC

Based on the results from the independence studies carried out for grid size, particles per cell, and time-step sizes, it was concluded to consider a domain with 20 particles per cell, a final grid size of $0.84\lambda \times 0.33\lambda$, and a time-step size of one-tenth of the mean collision time. Further sampling independence studies were carried out for different elapsed times like $\frac{100L_y}{c'} \leq t \leq \frac{300L_y}{c'}$ and $\frac{100L_y}{c'} \leq t \leq \frac{400L_y}{c'}$. Convergence of results was observed for both cases, and the final elapsed time of $\frac{100L_y}{c'} \leq t \leq \frac{300L_y}{c'}$ was considered for further simulations. A comparison of *μDSMC* results for center-line Mach number and normalized pressure with the standard DSMC [9] is highlighted in Figure 9a,b, respectively. Further, Figure 10 shows the radial variation in throat Mach number compared with that of standard DSMC [9] results.

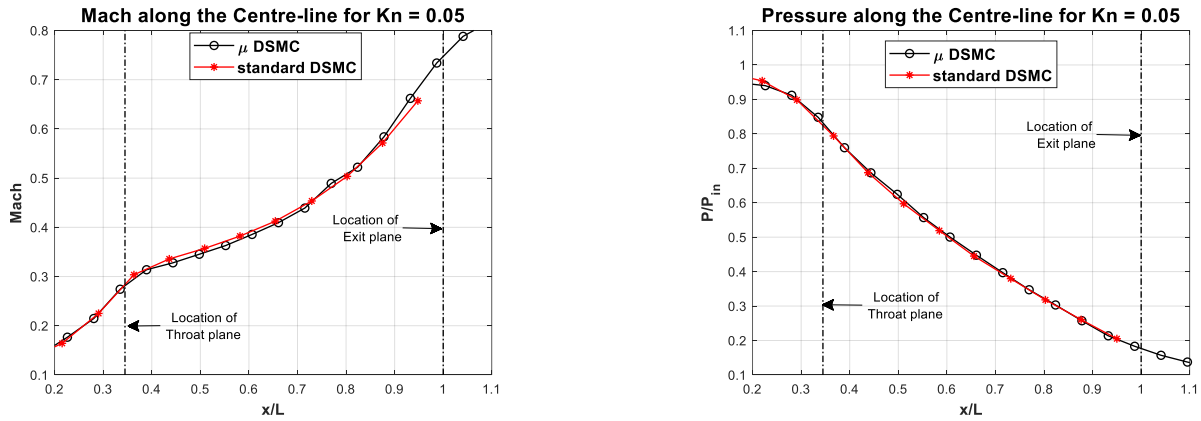


Figure 9. Comparison of results between *μDSMC* and standard DSMC for (**a**) center-line Mach number and (**b**) center-line normalized pressure.

It can be observed from Figures 9 and 10 that the *μDSMC* results are in close agreement with the standard DSMC [9] results. When the relative error was computed between the

said DSMC results, it was found to be less than 2.5% for the center-line Mach number and less than 1% for both the center-line normalized pressure ratio and throat Mach number.

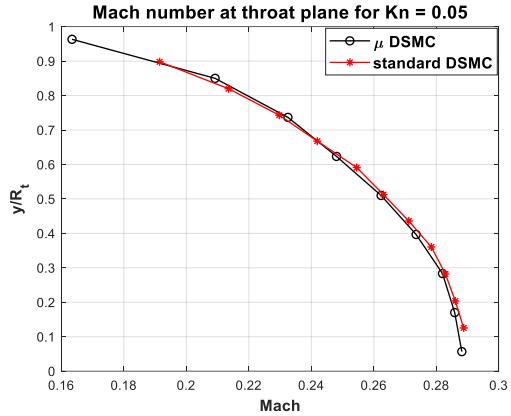


Figure 10. Comparison of throat Mach number between *μDSMC* and standard DSMC.

6. Flow Behavior in Micro-Nozzle

The micro-nozzle under discussion is shown in Figure 2 with the current flow conditions of an inlet pressure of 1576.8 Pa and inlet temperature of 300 K expanding into ambient conditions of 157.6 Pa with a wall temperature of 300 K. It can be observed from the variation in center-line Mach number shown in Figure 9a that the flow is un-choked through the nozzle. Due to rarefaction effects, the flow area is predominantly occupied by a viscous boundary layer which further affects the core flow gas properties of the nozzle. A few important performance parameters such as the effective exit flow ratio and specific impulse are defined. The core flow area is defined as an area having more or less uniform flow velocity, and the effective exit flow ratio is defined as the ratio of the core flow area at the exit to the geometrical area of the cross-section at the exit. This parameter highlights the portion of the area occupied by the boundary layer. A higher effective exit flow ratio implies a lower exit area being occupied by the viscous boundary layer. Specific impulse is defined as thrust delivered per unit weight flow rate through the nozzle, and this parameter is the most important performance parameter of any nozzle. With these parameters, flow behavior in a micro-nozzle is studied for different gas species and ambient pressures, as presented in the subsequent sections.

6.1. Study with Different Gas Species

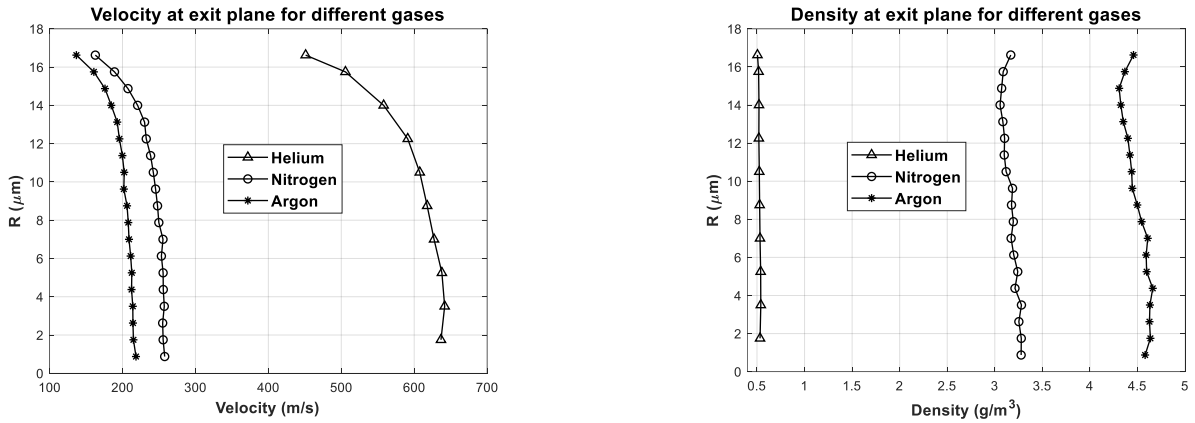
Flow behavior through the above-mentioned micro-nozzle is studied with different gas species such as helium, nitrogen, and argon. A similar study had been carried out by Roohi et al. [12] with nitrogen and argon expanding through a micro-nozzle. Simulations are carried out for the current flow conditions, and the gas properties considered are given in Table 2.

The radial variation in velocity and density at the exit plane for different gases is shown in Figure 11a,b, respectively. It can be inferred from Figure 11a that helium gas has a higher exit velocity and lower density than nitrogen and argon. When the flow Knudsen number was evaluated for the current flow conditions for the mentioned gases, helium was found to experience higher rarefied flow than argon and nitrogen with a Knudsen number of 0.16. Upon reviewing the results for exit velocity, the core flow area at the exit plane for helium was comparatively lower than that of nitrogen and argon due to higher rarefaction. In the case of helium, the exit area is predominantly occupied by a thicker boundary layer with an exit velocity higher than that of the remaining gases under consideration. Nozzle

performance parameters like the effective exit flow ratio and specific impulse are evaluated along with thrust and mass flow rate and are tabulated in Table 3.

Table 2. Properties of gases [14].

Parameters	Helium	Nitrogen	Argon
Molecular mass (kg)	0.665×10^{-26}	4.65×10^{-26}	6.63×10^{-26}
Molecular diameter (m)	2.53×10^{-10}	4.17×10^{-10}	4.17×10^{-10}
Rotational degrees of freedom	0	2	0
Viscosity exponent of gas	0.66	0.74	0.81
Sutherland constant (K)	79	111	144
Reference viscosity at 273 K (Ns/m^2)	1.897×10^{-5}	1.652×10^{-5}	2.125×10^{-5}



(**a**) (**b**)

Figure 11. Radial variation for different gases at exit plane: (**a**) velocity; (**b**) density.

Table 3. Performance parameters of micro-nozzle for different gas species.

Parameters	Helium	Nitrogen	Argon
Effective exit flow ratio (%)	17.0	67.8	76.6
Mass flow rate (μg/s)	0.259	0.654	0.781
Thrust (μN)	0.283	0.264	0.263
Specific impulse (s)	111.4	41.1	34.3

It can be inferred from the tabulated performance parameters that for nozzle flow, helium exhibits better efficiency in terms of thrust and specific impulse due to its low molecular weight. With argon, the nozzle had a higher mass flow rate, but the thrust delivered was comparatively the same as that of the nozzle with nitrogen, implying a lesser specific impulse for Argon. The effective exit flow ratio increased with gas molecular weight, but the achieved exit velocity was lower for gas with higher molecular weight. Due to this, the thrust of the micro-nozzle was reduced with gas molecular weight. It can be concluded that the nozzle will exhibit better efficiency with gas having a lower molecular weight in terms of thrust and specific impulse for the same operating conditions.

6.2. Study with Different Ambient Pressures

Flow expansion through the above-mentioned micro-nozzle is studied for different ambient pressures. The parameter back pressure ratio (*bPR*) is defined as the ratio of inlet

pressure to ambient pressure, and the simulations are carried out for different back pressure ratios varying from as low as 2 to as high as 20. Figure 12 highlights velocity contour plots for different back pressure ratios. It can be observed from Figure 12a that for a lower back pressure ratio of 2, flow velocity within the nozzle remained almost minimum within the nozzle. The variation in pressure along the center-line and radial variation in velocity at the exit plane for different back pressure ratios are shown in Figure 13a,b, respectively. It can be inferred from Figures 12a and 13a that nozzle flow expansion is ineffective for a back pressure ratio of 2, where flow velocity also was minimal within the nozzle.

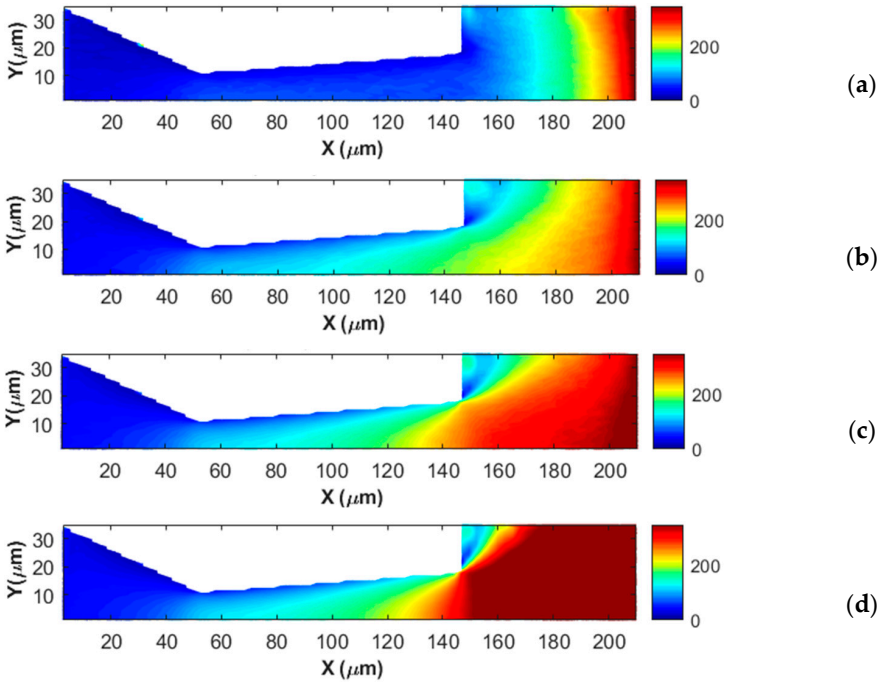
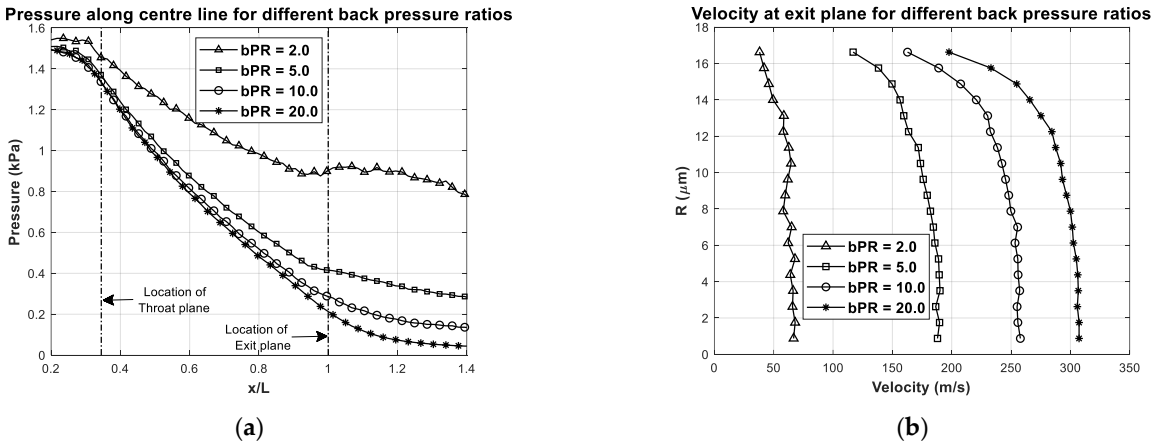


Figure 12. Velocity contours for different back pressure ratios: (**a**) bPR = 2, (**b**) bPR = 5, (**c**) bPR = 10, and (**d**) bPR = 20.



(**a**) (**b**)

Figure 13. Variation for different back pressure ratios: (**a**) center-line pressure; (**b**) velocity at exit plane.

The nozzle performance parameters like the effective exit flow ratio and specific impulse along with the delivered thrust and mass flow rate are evaluated for different back pressure ratios and tabulated in Table 4.

It can be observed from the tabulated values that the specific impulse, which is the main performance parameter of any nozzle, had increased with the back pressure ratio.

Further, as shown in Figure 13b, the velocity at the exit plane effectively increased as the back pressure ratio increased. When the core flow area at the exit was evaluated, it was observed that the effective exit flow ratio decreased with the back pressure ratio, which is due to the effect of the viscous boundary layer. Though the effective exit flow area is slightly lower at a higher back pressure ratio, the exit flow velocity is higher at the same ratio. Due to this, the thrust of the micro-nozzle increased with the back pressure ratio. For back pressure ratios of 5, 10, and 20, the mass flow rate through the micro-nozzle exhibits almost minimal variation but is higher than that for a back pressure ratio of 2, and hence, the specific impulse of the nozzle increased with the back pressure ratio. Further, it can be concluded from the performance parameters that the nozzle performed efficiently at higher back pressure ratios.

Table 4. Performance parameters of micro-nozzle for different back pressure ratios.

Parameters	bPR = 2	bPR = 5	bPR = 10	bPR = 20
Effective exit flow ratio (%)	85.8	76.6	67.8	51.9
Mass flow rate (μg/s)	0.426	0.625	0.654	0.666
Thrust (μN)	0.117	0.189	0.264	0.308
Specific impulse (s)	28	30.8	41.1	47.1

7. Conclusions

The viscosity-based DSMC approach (μDSMC), as proposed by Macrossan [3], has been implemented and extended to two-dimensional flows using the variable hard sphere collision model in a MATLAB platform. Boundary conditions for thermal slant walls and pressure boundaries at the upstream and downstream sections were applied. This study models nitrogen gas flow expansion through a micro-nozzle with a finite background pressure. To ensure numerical accuracy, grid independence studies were conducted by varying the axial grid size (Δx) and radial grid size (Δy). The results indicate that for reliable simulations, the radial grid size should be maintained at or below one-third of the local mean free path, while the axial grid size should not exceed the local mean free path. Time-step independence and particle count per cell were also analyzed, revealing optimal simulation conditions at a time step of one-tenth the mean collision time and a particle count of 20 particles per cell (*ppc*). The μDSMC approach demonstrated close agreement with standard DSMC results. Additionally, the influence of different gas species and varying back pressure ratios on micro-nozzle performance was examined. Important performance parameters like thrust, mass flow rate, and specific impulse were evaluated in terms of the effective exit flow ratio and exhaust velocity at exit. When micro-nozzle flow behavior was studied with different gas species at the same operating conditions, it was observed that with helium, the exit area of the nozzle was predominantly occupied by a viscous boundary layer due to a higher Knudsen number. In spite of this, the exit velocity was predominantly high with helium expanding through the micro-nozzle, and as a result, the thrust and specific impulse were also higher. When flow behavior was studied for different ambient pressures with nitrogen as a working gas, a parameter known as the back pressure ratio was defined, and it was observed that a minimum back pressure ratio (>5) needs to be maintained such that the nozzle expands effectively. It was also observed that as the back pressure ratio increased, the nozzle exit flow velocity increased, but at the expense of the effective flow area ratio being reduced. Further, the performance parameters such as thrust and specific impulse had increased with the back pressure ratio. In conclusion, nozzle efficiency is enhanced when a nozzle is operated at higher back pressure ratios, with helium being identified as a preferable choice for micro-nozzle expansion applications.

Author Contributions: Conceptualization, D.R.M., N.D. and S.P; methodology, D.R.M.; software, D.R.M.; validation, D.R.M., N.D. and S.P.; formal analysis, D.R.M.; investigation, D.R.M. and N.D.; resources, D.R.M. and S.P.; data curation, D.R.M.; writing—original draft preparation, D.R.M.; writing—review and editing, D.R.M. and N.D.; visualization, D.R.M.; supervision, N.D. and S.P. All authors have read and agreed to the published version of the manuscript.

Funding: This research received no external funding.

Data Availability Statement: Data is contained within the article.

Acknowledgments: The authors are deeply thankful to V K Saraswat (former SA to RM), B S Subhash Chandran (DRDO B D Nag Chaudari Chair), and M Raghavendra Rao (TBRL, DRDO) for extending their technical support in giving valuable suggestions for the current research work.

Conflicts of Interest: The authors declare no conflicts of interest.

Nomenclature

$\vec{c}$	Velocity vector of particle (m/s)
$\vec{c^*}$	Velocity vector of particle after collision (m/s)
$\vec{c'}$	Average thermal speed of molecule (m/s)
f_0	Maxwellian equilibrium distribution function
F_N	Statistical weight (No. of real gas particles represented by DSMC particle)
$\vec{g}$	Relative velocity between two chosen collision pair of particles (m/s)
k	Boltzmann's constant (J/K)
Kn	Knudsen number
L	Length of domain (m)
La	Mean free path (m)
m	Mass of gas molecule (kg)
n	Number density (molecules/m^3)
N_{coll}	Accepted number of collision pairs in a cell
N_{dsmc}	No. of DSMC particles in each cell
N_x	No. of cells in domain along axial direction
N_y	No. of cells in domain along radial direction
P	Gas pressure (Pa)
R	Characteristic gas constant (J/kg-K)
R_f	Random number uniformly distributed in [0, 1)
t	Current time (s)
T	Gas temperature (K)
$\overline{T}$	Time-averaged kinetic temperature (K)
T_s	Sutherland constant or measure of strength of attractive potential (K)
V	Volume (m^3)
(u,v,w)	Velocity components (m/s) along respective Cartesian directions
(x,y,z)	Cartesian coordinates
Γ	Gamma function
Δt	Discrete time step (s)
Δx	Axial grid size (m)
Δy	Radial grid size (m)
θ	Angle w.r.t axial direction (radian)
λ	Mean free path (m)
μ	Dynamic viscosity of gas (Ns/m^2)
ν	Constant related to viscosity exponent of gas
ρ	Gas density (kg/m^3)
σ	Total collision cross-section area (m^2)
ω	Viscosity exponent of gas
in	Inlet conditions

w	Wall conditions
e	Exit conditions
hs	Hard sphere molecule
vhs	Variable hard sphere molecule
N	Updated or new particle
$\perp$	Normal component of velocity
//	Parallel component of velocity
ref	Reference value
dsmc	DSMC particles
j	Cell index on boundary

Appendix A. DSMC Initialization and Basic Definitions

The viscosity of gas (μ_{in}) at inlet conditions can be evaluated from the available literature either using the Sutherland potential or the power law. Viscosity variation by Sutherland potential is given by Equation (A1):

$$\mu(T) = \mu_{ref}\left(\frac{T}{T_{ref}}\right)^{1.5}\frac{T_{ref}+T_s}{T+T_s} \tag{A1}$$

where T_s is a measure of the strength of the attractive potential and μ_{ref} is the reference viscosity of gas known at reference temperature T_{ref}. Viscosity variation by power law is given by Equation (A2):

$$\mu(T) = \mu_{ref}\left(\frac{T}{T_{ref}}\right)^{\omega} \tag{A2}$$

where ω is the viscosity exponent of the gas under consideration. For a hard sphere molecule, ω is 0.5, and for a variable hard sphere molecule, it is 0.74 in the case of nitrogen.

The choice of viscosity variation by Sutherland potential is more realistic and valid over a larger range of temperature when compared to that of power law variation, as it combines short-range hard sphere repulsion with a long-range inverse sixth-power attractive potential [3]. With known viscosity at inlet conditions, the mean free path for a hard sphere gas can be found and is given by Equation (A3):

$$\lambda_{hs} = \frac{16\mu_{in}}{5\rho_{in}}\frac{1}{\sqrt{2\pi RT_{in}}} \tag{A3}$$

The mean free path for variable hard sphere gas is given by Equation (A4):

$$\lambda_{vhs} = \frac{(7-2\omega)(5-2\omega)}{24}\lambda_{hs} \tag{A4}$$

Cell sizes in the domain are maintained as per Equation (A5).

$$0 < \Delta y \leq \frac{\lambda_{vhs}}{3} \tag{A5}$$

The number of cells in the computational domain axial direction (N_x) and radial direction (N_y) can calculated by Equation (A6)

$$N_x = \frac{L_x}{\Delta x}, N_y = \frac{L_y}{\Delta y} \tag{A6}$$

where L_x and L_y are the lengths of the computational domain in axial and radial directions, respectively.

The discrete time step is evaluated such that it is much less than the mean collision time. For a variable hard sphere collision model, the time step size is maintained as per Equation (A7).

$$\Delta t = 0.1\frac{\lambda_{vhs}}{\overline{c'}} \tag{A7}$$

where $\overline{c'}$ is the average thermal velocity of a molecule, as given by Equation (A8):

$$\overline{c'} = \sqrt{\frac{8RT_{in}}{\pi}} \tag{A8}$$

Appendix B. Brief on Diffusive Reflection for Thermal Wall

In diffusive reflection, the velocities of each reflected molecule are independent of its initial velocity. After a particle interacts with a moving or stationary thermal wall, reflected particle velocity components are reset according to biased Maxwellian distribution for normal components and standard Maxwellian Boltzmann distribution for parallel components. Distributions for velocity components are highlighted in Equations (A9) and (A10).

$$P(v_\perp) = \frac{1}{RT_w} v_\perp e^{-\left(\frac{v_\perp^2}{2RT_w}\right)} \tag{A9}$$

$$P(v_{//}) = \sqrt{\frac{1}{2\pi RT_w}} e^{-\left(\frac{v_{//}^2}{2RT_w}\right)} \tag{A10}$$

By simple inversion, generated velocities shall be obtained from Equations (A11) and (A12):

$$v_\perp = \sqrt{2RT_w}\sqrt{-\log R_f} \tag{A11}$$

$$v_{//} = \left(\sqrt{RT_w}\right) R_f \tag{A12}$$

where R_f is a random fraction uniformly distributed in [0, 1).

Based on the generated velocities, the updated position and velocity of the particle shall be decided based on the orientation and position of the wall.

- Horizontal Thermal Wall

For instance, the updated particle velocity upon interaction with a horizontal wall placed at a height of y_{wall} w.r.t origin is given by Equation (A13):

$$u_N = v_{//}; v_N = \pm v_\perp \tag{A13}$$

The updated position of the particle [11] is given by Equation (A14):

$$x_N = x; y_N = y_{wall} \pm |v_N| \left| \frac{y - y_{wall}}{v} \right| \tag{A14}$$

The sign shall be '+' for a bottom wall and '−' for a top wall in the domain.

- Vertical Thermal Wall

The updated particle velocity upon interaction with a vertical wall placed at a distance of x_{wall} w.r.t origin is given by Equation (A15).

$$u_N = \pm v_\perp; v_N = v_{//} \tag{A15}$$

The updated position of the particle [11] is given by Equation (A16):

$$x_N = x_{wall} \pm |u_N| \left| \frac{x - y_{wall}}{u} \right|; y_N = y \tag{A16}$$

The sign shall be '+' for a wall positioned on the left side and '−' for a wall positioned on the right side of the domain. If the wall is moving with a certain velocity, components of it shall be added to the respective updated particle velocities.

- Slant Thermal Wall

This is a special case of a thermal slant wall positioned at an angle 'θ_{wall}' w.r.t the 'x' axis and at the initial height of y_{wall} as shown in Figure A1. The distance of the interacting particle from the tip of the wall (having coordinates (x_{wall},y_{wall})) is 'AD', as given by Equation (A17):

$$AD = r = \sqrt{(x - x_{wall})^2 + (y - y_{wall})^2} \tag{A17}$$

And angle θ w.r.t the 'x' axis is given by Equation (A18):

$$\tan\theta = \frac{y - y_{wall}}{x - x_{wall}} \tag{A18}$$

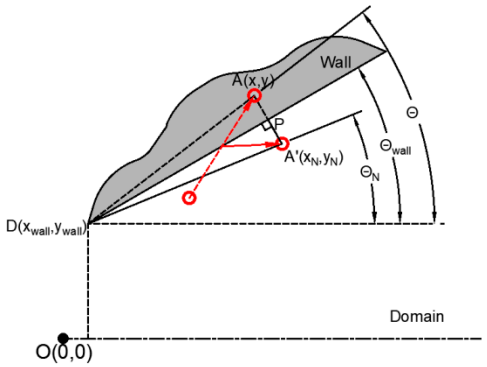


Figure A1. Diffuse reflection with thermal wall at the angle θ_{wall}.

The normal distance of the particle from the wall is 'AP', as given by Equation (A19):

$$AP = r\sin(\theta - \theta_{wall}) \tag{A19}$$

The time taken for the particle (dt) is considered as the ratio of the normal distance from the wall to the normal velocity component w.r.t the wall and is defined in Equation (A20):

$$dt = \left| \frac{AP}{u\sin\theta_{wall} - v\cos\theta_{wall}} \right| \tag{A20}$$

The updated normal distance of the particle from the wall inside the domain is given by Equation (A21):

$$PA' = v_{\perp} dt \tag{A21}$$

The updated distance of the particle from the tip of the wall is 'DB', as given by Equation (A22):

$$r_N = DA' = \sqrt{DP^2 + PA'^2} = \sqrt{(r\cos(\theta - \theta_{wall}))^2 + (v_{\perp} dt)^2} \tag{A22}$$

And the updated angle of the particle θ_N is given by Equation (A23):

$$\tan(\theta_{wall} - \theta_N) = \frac{PA'}{DP} = \frac{v_\perp dt}{r\cos(\theta - \theta_{wall})} \tag{A23}$$

So, the updated angle of particle w.r.t the 'x' axis can be evaluated and is given by Equation (A24):

$$\theta_N = \theta_{wall} - \tan^{-1}\left(\frac{v_\perp dt}{r\cos(\theta - \theta_{wall})}\right) \tag{A24}$$

As a result, the updated coordinates of the particle can be calculated as given by Equations (A25) and (A26):

$$x_N = x_{wall} + r_N \cos\theta_N \tag{A25}$$

$$y_N = y_{wall} + r_N \sin\theta_N \tag{A26}$$

The updated velocities of the particle can be evaluated as given by Equations (A27) and (A28):

$$u_N = v_{//}\cos\theta_w + v_\perp \sin\theta_w \tag{A27}$$

$$v_N = v_{//}\sin\theta_w - v_\perp \cos\theta_w \tag{A28}$$

Upon interaction with a thermal slant wall at an angle 'θ_{wall}' w.r.t the 'x' axis, the updated velocities and position of the particle will be evaluated as per Equations (A25)–(A28).

References

1. Bird, G.A. *Molecular Gas Dynamics and the Direct Simulation of Gas Flows*; Oxford university press: Oxford, UK, 1994.
2. Stewart, B.D.; Lumpkin, F.E. Axisymmetric Plume Simulations with Nasa's Dsmc Analysis Code. In Proceedings of the 33rd Exhaust Plume and Signatures (EPSS), Monterey, CA, USA, 3 December 2012.
3. Macrossan, M.N. μ-DSMC: A general viscosity method for rarefied flow. *J. Comput. Phys.* **2003**, *185*, 612–627. [CrossRef]
4. Wang, M.; Li, Z. Simulations for gas flows in microgeometries using the direct simulation Monte Carlo method. *Int. J. Heat Fluid Flow* **2004**, *25*, 975–985. [CrossRef]
5. Liou, W.W.; Fang, Y.C. Implicit boundary conditions for direct simulation Monte Carlo method in MEMS flow predictions. *Comput. Model. Eng. Sci.* **2000**, *1*, 119–128.
6. Yang, J.; Ye, J.J.; Zheng, J.Y.; Wong, I.; Lam, C.K.; Xu, P.; Chen, R.X.; Zhu, Z.H. Using direct simulation Monte Carlo with improved boundary conditions for heat and mass transfer in microchannels. *J. Heat Transfer. Apr.* **2010**, *132*, 041008. [CrossRef]
7. Shah, N.; Gavasane, A.; Agrawal, A.; Bhandarkar, U. Comparison of Various Pressure Based Boundary Conditions for Three-Dimensional Subsonic DSMC Simulation. *J. Fluids Eng.* **2018**, *140*, 031205. [CrossRef]
8. Hao, P.-F.; Ding, Y.-T.; Yao, Z.-H.; He, F.; Zhu, K.-Q. Size effect on gas flow in micro nozzles. *J. Micromechanics Microengineering* **2005**, *15*, 2069. [CrossRef]
9. Jaiswal, S.; Dongari, N.; Saraswat, V.K. Numerical Simulations of Rarefied Gas Flows in Micronozzles. Available online: https://scholar.google.com/citations?view_op=view_citation&hl=en&user=9Wxe8wwAAAAJ&cstart=20&pagesize=80&citation_for_view=9Wxe8wwAAAAJ:TQgYirikUcIC (accessed on 13 September 2024).
10. Macrossan, M.N. *Matlab Codes for the DSMC Calculation of Couette Flow, Using the Variable-Hard-Sphere (VHS) Collision Model*; University of Queensland: Brisbane, Australia, 2009.
11. Garcia, A.L. *Numerical Methods for Physics*; Prentice Hall: Englewood Cliffs, NJ, USA, 2000.
12. Saadati, S.A.; Roohi, E. Detailed investigation of flow and thermal field in micro/nano nozzles using Simplified Bernoulli Trial (SBT) collision scheme in DSMC. *Aerosp. Sci. Technol.* **2015**, *46*, 236–255. [CrossRef]
13. Xie, C. Characteristics of micronozzle gas flows. *Phys. Fluids* **2007**, *19*, 037102. [CrossRef]
14. White, F.M.; Majdalani, J. *Viscous Fluid Flow*; McGraw-Hill: New York, NY, USA, 2006; Volume 3.

Disclaimer/Publisher's Note: The statements, opinions and data contained in all publications are solely those of the individual author(s) and contributor(s) and not of MDPI and/or the editor(s). MDPI and/or the editor(s) disclaim responsibility for any injury to people or property resulting from any ideas, methods, instructions or products referred to in the content.